Bulletin of the Seismological Society of America, Vol. 95, No. 5, pp. 1856–1864, October 2005, doi: 10.1785/0120040185

Space–Time Clustering of Large Thrust Earthquakes along the Mexican Subduction Zone: An Evidence of Source Stress Interaction

by Miguel A. Santoyo, Shri K. Singh, Takeshi Mikumo, and Mario Ordaz

Abstract The spatiotemporal plot of epicenters of large ($M_s \geq 6.9$) subduction earthquakes in Mexico (1900 to present day) suggests that these earthquakes cluster in space and time. In this work we test the hypothesis that the coseismic stress transfer may lead to this clustering. For the analysis we estimate the spatial extent of the coseismic Coulomb stress change for these large events and then perform a statistical analysis using the χ^2 goodness-of-fit test for the interevent time intervals. We find that there are, at least, two groups of time intervals where the observed frequencies are much higher than that expected from a Poisson model, indicating a bimodal pattern. For the first mode, the observed frequencies for the 0- to 5-year interval becomes about 2.1 times the expectation, with a probability of occurrence of about 30%. These results show that large thrust Mexican earthquakes between 1900 and 2003 are clustered in space and time probably due to stress interactions among them. The second mode includes the time interval of 30–50 years. In the interval of 30–40 years, the observed frequencies become about 1.7 times the expectation and about 1.2 times the expectation for the 40- to 50-year interval. This second mode could be associated with a reloading interval of tectonic stress due to the plate convergence and appears consistent with the long-term recurrence periods of large thrust earthquakes in the Mexican subduction zone.

Introduction

A glance at the spatiotemporal plot of epicenters of large subduction earthquakes in Mexico, which occurred during the last 103 years on the Pacific coast, suggests that these events are clustered in space and time (e.g., Singh *et al.*, 1981; Nishenko and Singh, 1987a; Ward, 1991). Several authors have reported a positive correlation between the coseismic stress changes on the neighborhood of the source region, and the occurrence in clusters of subsequent earthquakes with different magnitudes in the same area (e.g., King *et al.*, 1994; Stein *et al.*, 1994; Deng and Sykes, 1997; Freed and Lin, 1998; Gomberg *et al.*, 1998; Harris, 1998, Toda *et al*, 1998; Stein, 1999). Here, the term stress transfer or earthquake interaction implies that given an earthquake, the time of occurrence of the following large events in its close neighborhood is accelerated in time due to its coseismic stress increase outside the main slip region.

In this study, we test the hypothesis that the coseismic stress transfer leads to clustering of large thrust earthquakes in the Mexican subduction zone. For this purpose, we define a criterion to obtain the interoccurrence times, taking into account the spatial extent of the changes of the Coulomb failure stress due to the coseismic slips of each earthquake. The analysis is performed with the aid of the Pearson χ^2 statistical test, with reference to a Poisson model of earthquake occurrence as our null hypothesis. For this purpose, we analyze the Mexican earthquake catalog from 1900 to 2003.

Earthquake Data

The Mexican earthquake catalog is complete from 1900 to the present for events with magnitudes $M_s \geq 6.5$ (Singh *et al.*, 1984; Kostoglodov and Pacheco, 1999). As our method is based on the spatial relationship between large earthquakes, we only consider rupture areas greater than 625 km^2 (25 km $\times$ 25 km), which is equivalent to events with $M_s \geq 6.9$. The catalog for this period and magnitudes comprises 46 shallow thrust earthquakes (Table 1).

Method of Analysis

Rupture Areas

The rupture areas for each earthquake are estimated from their aftershock areas when they are known. The aftershock areas have been mapped for only 24 out of the 46 events (Fig. 1, Table 1). For the remaining events, we estimate the rupture area from an empirical relation: $\log(S) = M_s - 4.1$ (e.g., Utsu and Seki, 1954; Purcaru and Berck-

Table 1
Catalog of Shallow Thrust Mexican Earthquakes with Magnitudes $M_s \geq 6.9$ (1900–2003)

Event No.	Date (yr/dd/mm)	Location* Lat.	Location* Lon.	$M^{\dagger}$	$L^{\ddagger}$	Event No.	Date (yr/dd/mm)	Location* Lat.	Location* Lon.	$M^{\dagger}$	$L^{\ddagger}$
1	1900/1/20	20.0	−105.0[1]	(7.6)[2]	79.5[3]	24	1941/4/15	18.85	−102.94[1]	(7.9)[1]	112.3[3]
2	1900/5/16	20.0	−105.0[1]	(7.1)[2]	44.7[3]	25	1943/2/22	17.62	−101.15[1]	(7.7)[1]	89.2[3]
3	1907/4/15	[16.62]	[−99.2][4]	7.9[4]	150.6[4]	26	1950/12/14	[16.61]	[−98.82][4]	7.3[7]	58.2[4]
4	1908/3/26	16.7	−99.2[5]	(7.8)[2]	100.1[3]	27	1957/7/28	[16.59]	[−99.41][4]	7.8[7]	92.0[4]
5	1908/3/27	17.0	−101.0[5]	(7.2)[2]	50.2[3]	28	1962/5/11	[16.93]	[−99.99][9]	7.1[9]	40.0[9]
6	1908/10/13	18	−102.0[5]	(6.9)[5]	35.5[3]	29	1962/5/19	[16.85]	[−99.92][9]	7.0[9]	35.0[9]
7	1909/7/30	16.8	−99.9[1]	(7.5)[2]	70.9[3]	30	1965/8/23	[15.58]	[−96.02][10]	7.5[7]	108.5[10]
8	1909/7/31	16.62	−99.45[1]	(7.1)[2]	44.7[3]	31	1968/8/2	[16.01]	[−98.01][10]	7.3[7]	70.0[10]
9	1909/10/31	17.1	−101.1[1]	(6.9)[2]	35.5[3]	32	1973/1/30	[18.29]	[−103.41][11]	7.7[11]	90.0[11]
10	1911/6/7	17.5	−102.5[6]	(7.9)[6]	112.3[3]	33	1978/11/29	[15.75]	[−97.05][10]	7.8[12]	84.0[10]
11	1911/12/16	17	−100.7[1]	(7.6)[2]	79.5[3]	34	1979/3/14	[17.46]	[−101.45][13]	7.4[12]	95.0[13]
12	1928/3/22	15.67	−96.1[7]	(7.5)[6]	70.9[3]	35	1981/10/25	[17.75]	[−102.25][14]	7.2[12]	48.0[14]
13	1928/6/17	15.8	−96.9[1]	(7.8)[6]	100.1[3]	36	1982/6/7–1	[16.35]	[−98.37][15]	6.9[12]	53.0[15]
14	1928/8/4	16.1	−97.4[1]	(7.4)[6]	63.2[3]	37	1982/6/7–2	[16.4]	[−98.54][15]	6.9[12]	57.0[15]
15	1928/10/9	16.3	−97.3[1]	(7.6)[6]	79.5[3]	38	1985/9/19	[17.79]	[−102.51][16]	8.1[12]	180.0[16]
16	1932/6/3	[19.8]	[−105.4][8]	8.0[7]	222.0[8]	39	1985/9/21	[17.62]	[−101.82][16]	7.5[12]	80.0[16]
17	1932/6/18	[18.99]	[−104.6][8]	7.9[7]	71.0[8]	40	1986/4/30	[18.42]	[−102.49][16]	6.9[12]	55.0[16]
18	1932/6/22	18.74	−104.68[8]	(6.9)[8]	35.5[3]	41	1989/4/25	[16.58]	[−99.46][17]	6.9[12]	35.0[17]
19	1932/7/25	18.87	−103.93[8]	(6.9)[8]	35.5[3]	42	1995/9/14	[16.48]	[−98.76][18]	7.3[12]	45.0[18]
20	1933/5/8	17.5	−101.0[1]	(6.9)[1]	35.5[3]	43	1995/10/9	[19.1]	[−104.90][19]	8.0[12]	175.0[19]
21	1934/11/30	19	−105.31[8]	(7.0)[8]	39.9[3]	44	1996/2/25	[15.78]	[−98.26][20]	7.1[12]	68.0[20]
22	1935/6/29	18.75	−103.5[8]	(6.9)[8]	35.5[3]	45	2000/8/9	17.99	−102.66[21]	(6.9)[3]	35.5[3]
23	1937/12/23	[16.39]	[−98.61][4]	7.5[7]	61.2[4]	46	2003/1/22	[18.7]	[−104.20][22]	7.6[12]	72.0[22]

*Bracketed numbers indicate the location of the center of the rupture area.

$^{\dagger}M = M_s$ if in parenthesis, otherwise $M = M_w$.

‡L indicate the lengths of the faults along the coast (see text).

Numbers shown as superscripts indicate references: 1, Singh *et al.* (1984); 2, Nishenko and Singh (1987a); 3, L from $\log(S) = M_s - 4.1$; 4, Nishenko and Singh (1987b); 5, Singh *et al.* (1981); 6, Anderson *et al.* (1989); 7, Singh and Mortera (1991); 8, Singh *et al.* (1985); 9, Ortiz *et al.* (2000); 10, Singh *et al.* (1980); 11, Reyes *et al.* (1979); 12, Harvard CMT catalog; 13, Valdés and Novelo (1998); 14, Havskov *et al.* (1983); 15, Astiz and Kanamori (1984); 16, UNAM seismology group (1986); 17, Zuñiga (1993); 18, Courboulex *et al.* (1997); 19, Pacheco *et al.* (1997); 20, Santoyo and Islas, unpublished report; 21, SSN catalog; 22, Singh *et al.*, 2003.

hemer, 1978; Wells and Coopersmith, 1994), where S is the source area in km^2, and M_s is the surface-wave magnitude. During the period considered here, there are four earthquakes of magnitude M_w 6.9 with known aftershock areas. All of them show an aspect ratio of about $L = W$ (see Fig. 1), where L is the length along the strike direction and W is the width along the dip direction, L being the horizontal distance of the estimated source area S. From this observation, we assume that the remaining 6.9 earthquakes on the catalog behave approximately in the same way. For the events with magnitudes over 7.0 with known aftershock areas, they show aspect ratios between $1.5 < L/W < 3.0$ (Fig. 1), so we assume an aspect ratio of $L = 2W$ for them.

Interevent Times

It is critical to establish the rule by which the interoccurrence times between earthquakes will be determined. One possibility is to take the earthquake catalog in a region and a minimum threshold magnitude and to calculate the time difference between subsequent events as they appear in the catalog. Since this method does not take into account the spatial distance between the events, one could be accounting for the time interval between two earthquakes that could be several hundreds of kilometers apart from each other.

Our criterion to obtain the interevent times specifically consists of the following: We first select, from the catalog, the earthquake that occurred first in time and estimate the possible extent of the zones of coseismic increase in the Coulomb failure stress (ΔCFS) from the rupture area, as described in the next section. Second, from all the rupture areas for subsequent events, we look for the first event in time that spatially overlaps the zone of stress increase due to the specified earthquake, and then take the time interval between them if they actually overlap. Third, because this spatial overlapping could be only partial, we check if the zone of stress increase is completely overlapped by the fault area of the second event. If not, we take the remaining nonoverlapped region, and continue searching for the next consecutive earthquake whose fault area spatially overlaps the remaining region. Then, we take again the interevent time between the first specified and third events. In this way, the procedure is repeated until the entire region of stress increase due to the specified earthquake is fully overlapped. We consider in this procedure that an earthquake can produce a stress influence on more than one earthquake in the future

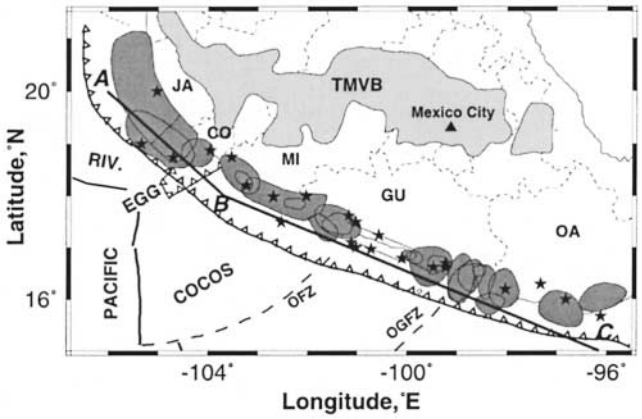

Figure 1. Tectonic map of Mexico. Gray areas show the aftershock area of large earthquakes from 1900 to 2003. Stars represent the epicentral locations of earthquakes for which there are no aftershock areas available. Thin lines parallel to the coast show the spatial extent of the sequence 1908–1911 in Guerrero. The solid line ABC is the reference line for the projection of these events. TMVB, Trans-Mexican Volcanic Belt; OFZ, Orozco Fracture Zone; OGFZ, O'Gorman Fracture Zone; EGG, El Gordo Graben; PACIFIC, COCOS, RIV, Pacific, Cocos and Rivera oceanic plates, respectively; JA, Jalisco; CO, Colima; MI, Michoacan; GU, Guerrero; OA, Oaxaca.

and also that a given earthquake can be influenced by more than one event in the past. We also assume that all the stress accumulated due to an earthquake in the overlapped zone will be released by the next events.

The above method is recursively applied to the time for each earthquake in the catalog, until the entire time period of the catalog is analyzed. This procedure provides a set of interevent times between earthquakes that are now related in the spatial domain. In a later section we show a detailed example of this procedure.

After this is done, the interevent times are analyzed by the aid of the χ^2 statistical test, with reference to a Poisson model of occurrence. We analyze two sets of interevent times: the set **A**, obtained by the method proposed above, which takes into account the stress interaction between earthquakes, and another set **B**, obtained from the time difference between subsequent events directly as they appear in the catalog.

Coulomb Failure Stress

For the computation of the Coulomb failure stress change, we used the relation $\Delta CFS = \Delta\tau + \mu'\Delta\sigma_n$ (e.g., Harris, 1998), where $\Delta\tau$ is the shear stress change in the direction of the fault slip, $\Delta\sigma_n$ is the change in the tensional stress normal to the fault plane, and μ' is an apparent coefficient of friction $\mu' = \mu\ (1 - p)$, where μ is the static coefficient of friction and p is the pore pressure in the source volume. In this study, we used the formulations given by Okada (1985, 1992) to compute the coseismic ΔCFS in a 3D tensorial way. In the computations, we used a shear modulus of $\mu = 3.5 \times 10^{11}$ (dyne cm^2), with a Poisson ratio of $\nu = 0.25$. For the tectonic apparent coefficient of friction, we used the value of $\mu' = 0.4$ adopted by Mikumo *et al.* (1999, 2002) for the Mexican subduction zone.

As all the thrust earthquakes considered in this study occur on the upper plate interface between the North-America Plate and the Rivera or Cocos Plates (see Fig. 1), the ΔCFS function is computed on this fault interface with the average direction of faulting motion. For the Mexican subduction zone, we used the average parameters: $\delta = 15°$ (dip), and $\lambda = 90°$ (slip). The strike is assigned depending on the subducting plate. In the case of the Rivera plate, we used a strike of $\theta_r = 300°$, and for the Cocos plate we used $\theta_c = 290°$.

To define the spatial extent of coseismic stress increase that would affect future earthquakes, we tentatively take the area whose ΔCFS brings the adjacent region at least 1.0 bar (0.1 MPa) closer to the failure. Values of this order have been recognized by different authors to have effective influence on the neighborhood seismicity around the fault area (e.g., King *et al.*, 1994; Hardebeck *et al.*, 1998; Harris, 1998; Stein, 1999).

Earthquakes have a heterogeneous slip distribution over the fault plane. Unfortunately, this information is available only for some recent Mexican earthquakes. Due to this limitation, we assumed an elliptical distribution of slip over the fault, tapered with a cosine function of 15% for all events (Fig. 2a), which is expected from a nearly uniform stress drop. As we discuss in a next paragraph, this assumption does not significantly affect the estimation of the ΔCFS on the extended plane.

Using this model for earthquakes with magnitudes between M_w 7.0 and M_w 8.0 and a mean depth of 20 km, the area with $\Delta CFS \geq +1.0$ bar is found to be about four to five times the original fault area. This means that the length of this area along the trench is about twice the fault length (see Fig. 2b, c). In this study we call this length the distance of effective influence (DEI). Note that the values of ΔCFS outside the ruptured fault area are positive when computed over the extended fault plane, and nonuniform negative values inside the fault area. In general, actual earthquakes have also some positive ΔCFS zones inside the fault area due to heterogeneous slip distribution. Due to this, in our analysis we consider the fault rupture length as a portion of the DEI.

Figure 3 shows the space–time plot of all the selected earthquakes for this study. The x axis (abscissa) is the distance along the trench, taken along the line ABC shown in Figure 1, which is approximately parallel to the trench. The y axis (ordinate) represents time in years, beginning in 1900. The earthquake fault zones are projected onto the line ABC and are shown as horizontal lines where their ordinate value is the date of their occurrence. Thick solid lines represent the fault extent of each earthquake in the direction parallel to the trench, and thin lines denote the spatial extent of their stress influence (the DEI length) projected onto line ABC.

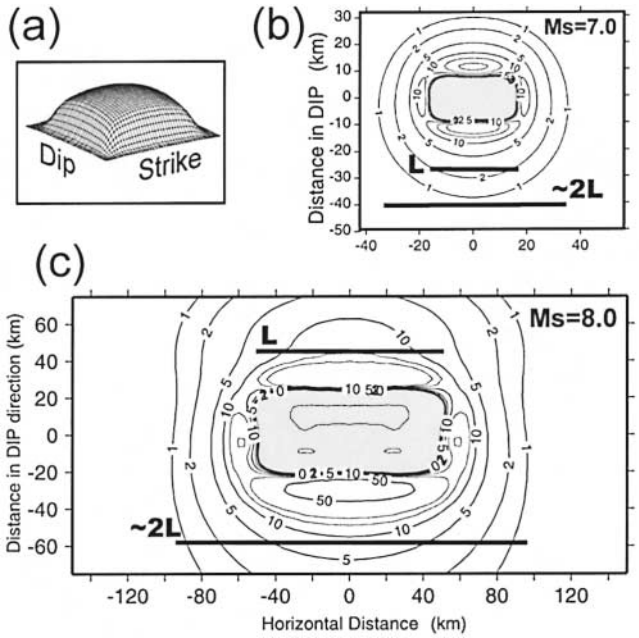

Figure 2. ΔCFS from two possible earthquakes over their extended fault plane. The stress changes are given in bars. The aspect ratio of the fault size is $L = 2W$ for the two assumed events. For this model, we take dip = 15°, slip = 90°, and the center of the fault is located at a depth of 20 km. (a) The slip is assumed to have an elliptical distribution with a cosine tapering of 15% over the length and width. (b) An earthquake with a moment magnitude M_w 7.0. (c) An earthquake with M_w 8.0. Note that the horizontal distance between +1 bar contours on the extended plane is approximately twice the assumed fault length (L).

In Figure 4 we show an example of the method to obtain the interevent times from the space–time plot in Figure 3. Here, we take a subcatalog of eight earthquakes that occurred between 1900 and 1945 and between 400 and 700 km along the projection line ABC. We begin with the DEI of earthquake A (27 March 1908), as it is the first to appear in the subcatalog (Fig. 4a). The next earthquake to appear in time on the catalog is event B (13 October 1908), but its rupture area does not overlap the DEI of event A, so the time interval between them is not taken into account. The next earthquake to appear in time is event C (31 October 1909). In this case, its rupture area partially overlaps the DEI of event A, so the time interval Δ1 between them is taken into account. However, since event C does not overlap the entire DEI length of A, we continue searching for the next consecutive earthquake whose fault area spatially overlaps the remaining region. Here event D (7 June 1911) does not overlap the DEI of A, but event E (16 December 1911) does, so we take the time Δ2 between A and E. Event F (8 May 1933) again overlaps a small part of the remaining region, so we take the time interval Δ3. In the same sense, only event H (22 February 1943) and not event G (15 April 1941), overlaps the remaining region of A, so we take only Δ4 between A and H. Now the DEI of A is completely overlapped by the four events. We repeat the procedure with the DEI of the next event B. Here, event D is the only one to overlap the DEI of B, so in this case we only take the time interval Δ5 (Fig. 4b). Following the same procedure, in Figure 4c, we find that only events E, F, and H overlap the DEI of C, so we take the times Δ6, Δ7, and Δ8, respectively. Figure 4d shows that for event D, only G and H overlap its DEI so we take the time intervals Δ9 and Δ10. In this example we can observe that one earthquake can influence more than one event in the future and that a given earthquake can be influenced by more than one event in the past.

A more detailed analysis using actual slip distributions over the fault plane will not necessarily produce a significant difference on the DEI obtained by our method. The Coulomb stress changes outside the rupture fault area are not very sensitive to the slip distribution inside the fault area. Variations of the slip are significant only inside the source area, in the sense that as one goes away from the main slip zone, the ΔCFS represents the result due to the sum of the mean slip variations. In order to check this assumption, we performed tests to compare the variations in the ΔCFS outside the main fault area, assuming an elliptical slip distribution, with those from the slip distributions obtained by kinematic waveform inversion of three earthquakes: the 19 September 1985 M_s 8.1, Michoacan (Mendoza and Hartzell, 1989), the 14 September 1995 M_s 7.3 Copala (Courboulex *et al.* 1997), and the 25 April 1989 M_s 6.9, San Marcos (Santoyo, 1994; Zuñiga *et al.*, 1993) earthquakes. The results on DEI differ only by 15%. Further tests described in the Appendix show that these variations in the DEI do not significantly affect the final results.

There is a possibility, however, that the absolute value of ΔCFS would become somewhat larger if some difference in elastic properties between the crust overriding the subducting plate and those inside the plate is taken into account, and hence that the DEI would become slightly larger. In a more detailed analysis, it would also be necessary to incorporate postseismic stress variations due to plate convergence and viscoelastic relaxation process (e.g., Mikumo *et al.*, 2002).

Results from Statistical Analysis and Discussion

Following the method outlined earlier, we obtained 113 interevent times for the set of 46 earthquakes. A statistical analysis of these interevent times is now performed by the aid of the χ^2 test for the goodness of fit (e.g., Benjamin and Cornell, 1970). Our working hypothesis is that the interevent times (**A**) obtained by our method would differ significantly from a Poisson process, showing a clustering behavior.

To ensure that our results are due to earthquake interactions and not simply to the time distribution of the earthquakes in the catalog, we also analyzed the set of interevent times (**B**) taken simply from the time difference between

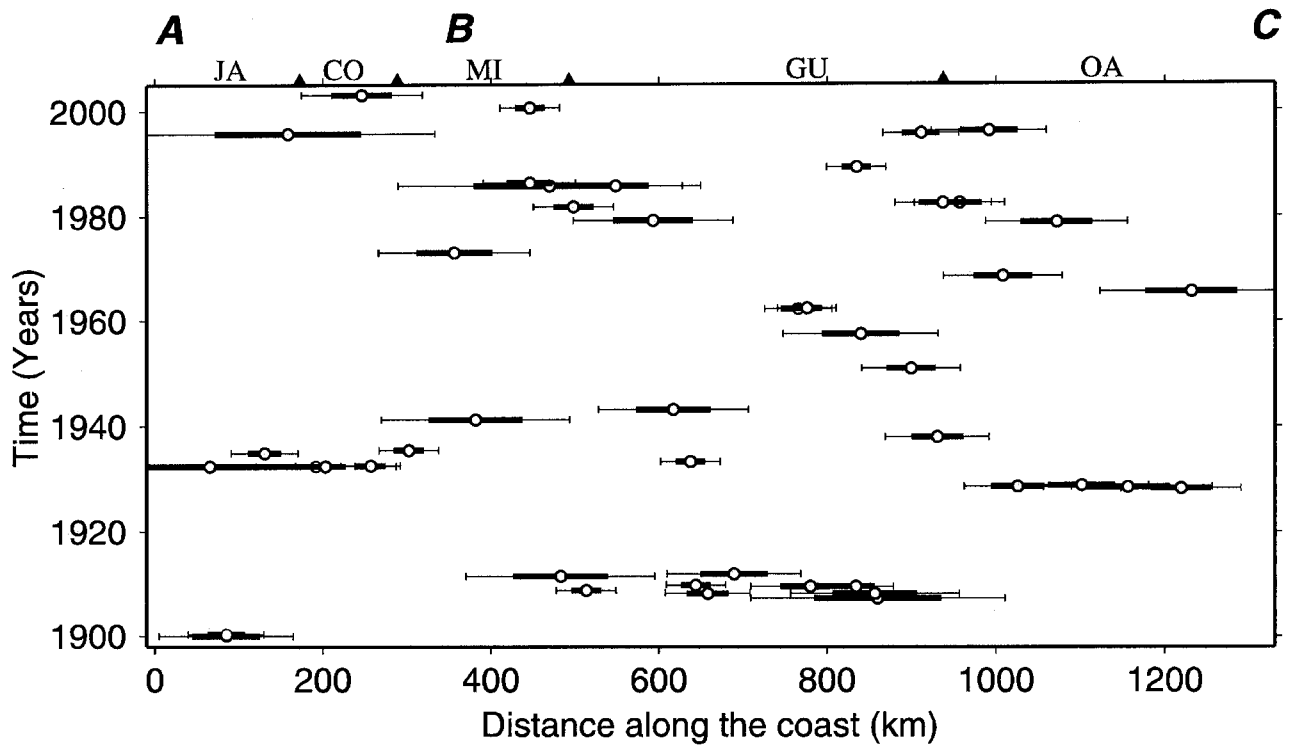

Figure 3. Space–time plot of the Mexican subduction earthquakes with $M_s \geq 6.9$, taken from the catalog for the period from 1900 to 2003. The abscissa is the distance in kilometers along the projection line ABC shown in Figure 1. A and C are located at the northwestern and southeastern ends of the projection line. The ordinate represents time in years beginning at 1900. Open circles indicate the epicentral location projected onto the line ABC at the occurrence time of earthquakes. Thick and thin horizontal lines represent the source length (L) and the DEI of each earthquake, respectively, projected along the line ABC. JA, CO, MI, GU, and OA same as in Figure 1.

subsequent events as they appear in the catalog. In this case, the χ^2 test is expected to favor the null hypothesis, showing a Poisson behavior.

The interevent time intervals (**A**) obtained by our method are grouped into two class intervals (5 and 10 years) taking care of having no less than 5 elements in each interval, and the data are analyzed for the 99% and 99.9% significance levels (Benjamin and Cornell, 1970). The results are summarized in Table 2. For the two different selections of class intervals, the results do not allow us to reject the working hypothesis of earthquake clustering, on the ground that the test results are greater than both of the 1.0% and 0.1% χ^2 distribution percentage points (Abramowitz and Stegun, 1972), as seen in Table 2. To assure that our method would not identify an unclustered dataset as a clustered one, we performed the test which is explained in detail in the appendix. Also in the appendix we performed another test of the effects of changing 15% the length of the DEI.

In Figure 5a it can be observed that once an earthquake has occurred, approximately 30% of the subsequent events occur in the next 5 years, possibly due to the stress interactions.

The next set of time intervals (**B**) taken directly from the catalog was grouped into the class interval of 5 years, using the same procedure as for the previous set **A**. The results from the χ^2 test for this case are summarized in Table 2. Here the results do not allow us to reject the null hypothesis, showing that these interevent times follow a much more random behavior.

In Figure 5b and c it can be observed that there are two groups of time intervals where the observed frequencies of occurrence are much higher than those expected from the Poisson model, indicating a bimodal pattern. This behavior could be divided into a short-term mode of clustering of events and a long-term mode for recurrence-type period for large earthquakes.

The first group of intervals, or the first mode, falls between 0 and 5 years, where the observed frequencies are approximately two times higher than that expected from the Poisson model. The second group of intervals, or the second mode, falls between 30 and 50 years, and the observations are about two times the Poisson's expectation.

These results imply that just after the first year of the occurrence of a large earthquake, the probability of occurrence of another large event in the same region is much higher than that expected from a random process, and that

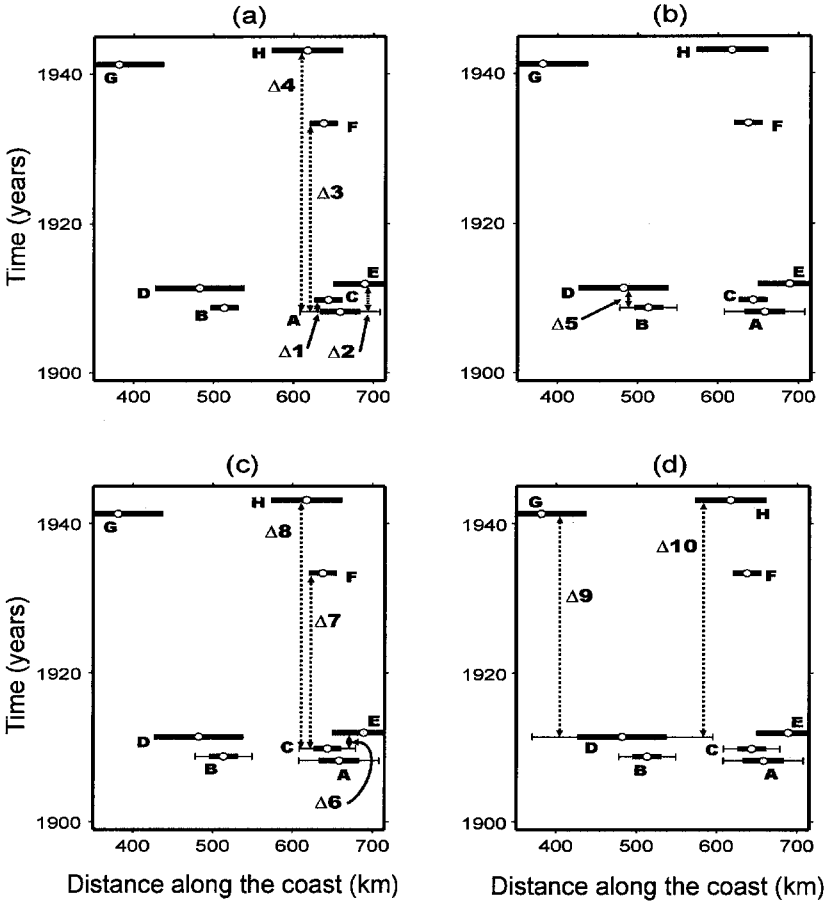

Figure 4. Example of the method used to obtain the interevent times, based on the spatial extent of the coseismic Coulomb failure stress. Rupture areas projected on line ABC of Figure 1 are shown as thick solid lines. Earthquakes: A, 27 March 1908; B, 13 October 1908; C, 31 October 1909; D, 7 June 1911; E, 16 December 1911; F, 8 May 1933; G, 15 April 1931; H, 22 February 1943; see Table 1 for details. The extent of the DEI of events A, B, C, and D, are shown as thin solid lines. (a) Time intervals counted from event A; (b) time intervals counted from event B; (c) time intervals counted from event C; (d) time intervals counted from event D. See text for the description of the method.

Table 2
Results for the Statistical Analysis of Interevent Times

Data Set	Class Int. (Years)	Test Results	χ^2 99%*	χ^2 99.9%†	Allow to Reject Null Hypothesis
A	5.0	73.3	36.19	43.82	Yes
	10.0	38.73	21.67	27.88	Yes
B	5.0	0.88	6.63	10.83	No

*Values for the 1.0% percentage points (Abramowitz and Stegun, 1972).
†Values for the 0.1% percentage points (Abramowitz and Stegun, 1972).

in the interval 0–5 years, the probability of occurrence due to the interaction between large earthquakes is near 35%.

The second mode (30–50 years) could be associated with the reloading interval of tectonic stress due to the plate convergence. In fact, these results do not appear inconsistent with the analysis of recurrence times based on the seismic gap hypothesis. Nishenko and Singh (1987a) found that in the Mexican subduction zone, the long-term recurrence time for earthquakes with magnitudes $M_s \geq 7.5$ varies from 28 to 54 years, with a mean of about 40 years. Using a different method than Nishenko and Singh (1987a), Zuñiga and Wyss (2001) also observed recurrence times of these orders (20–40 years) in the southern portion of the Mexican subduction zone. The second mode of our results indicates that the lobe in the frequencies of occurrence between 30 and 50 years could be associated with the long-term recurrence periods found by Nishenko and Singh (1987a), Zuñiga and Wyss (2001), and others.

Even though these results are not inconsistent with the analyses by the seismic gap theory for long-term recurrence periods, there is an important group of large events that occur soon after the occurrence of large earthquakes. Thus, special care should be taken in relation to the time periods after a large earthquake have occurred, especially for seismic hazard analyses for large subduction earthquakes in Mexico.

On 22 January 2003, a large earthquake with magnitude M_w 7.6 occurred in front of the coast of the Mexican state of Colima, at the southeast end of the 9 October 1995, M_w 8.0, Jalisco earthquake fault (Singh *et al.*, 2003; Yagi *et al.*, 2004) (Table 1). This earthquake occurred just in the area of the effective stress influence from the 1995 Jalisco earthquake, eight years after its occurrence, and also from the 1973 earthquake, almost 30 years after the event (Fig. 3). In agreement with our results and the results by other authors, this could be an indication that the last event has influenced the occurrence of a next event with a positive ΔCFS, incrementing the rate of seismicity in its adjacent zones. Under our scheme, given the 1995 earthquake, the probability of occurrence of the 2003 event in its area of

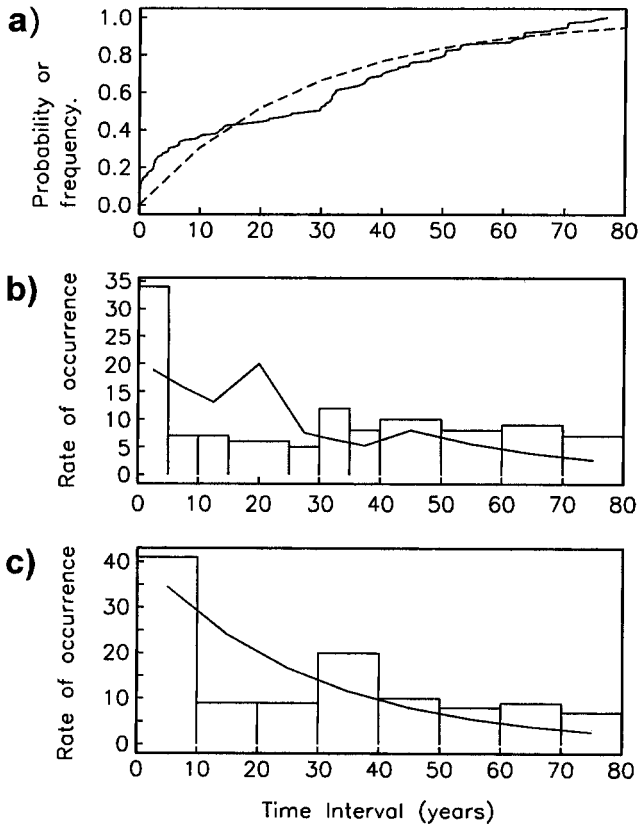

Figure 5. Histograms of interevent times and probabilities. (a) Normalized acumulated frequency of set **A** (solid line) and that expected from the Poisson model (dashed line). (b) Results obtained by the method proposed in this study (set **A**) for a time interval of 5 years, combining bins where raw data contains less than five elements. Continuous lines here are the curves for the expected values from a Poisson model of occurrence. (c) Same as (b) for a time interval of 10 years.

positive effective stress influence, was about 36% after eight years, as shown in Figure 5a. This value is about twice that expected from the Poisson model.

Conclusions

Several studies have shown that the clustering of earthquakes is not restricted to aftershock or foreshock sequences, but also occurs for large and great earthquakes (e.g., Kagan and Knopoff, 1976; Kagan and Jackson, 1991). Our study shows that the probable stress interaction in a group of large thrust earthquakes ($M_w \geq 6.9$) in the Mexican subduction zone is leading to their clustering behavior in space and time. It also shows that this behavior is not simply due to the temporal distribution of the large earthquakes itself on the catalog.

We find that given a large earthquake ($M_w \geq 6.9$), the probability of occurrence of another large event in the same region is much higher than that expected from a random process. In the interval of 0 to 5 years, the probability of occurrence of another large earthquake in the neighboring region is about 30%, about twice that expected from a Poisson model. The results of our analysis should be taken into account in earthquake forecast and seismic hazard estimation in Mexico.

On the other hand, it is necessary to perform a more detailed analysis in a three-dimensional scheme to account for the interevent times due to the stress interaction between shallow-thrust and in-slab normal faulting earthquakes in this subduction zone.

Acknowledgments

The authors wish to acknowledge fruitful discussions with Javier Pacheco. The Coulomb failure stress computations were performed using the code DIS3D. We thank two anonymous reviewers and Stefan Wiemer for their critical comments. This work was partially supported by DGAPA, UNAM Project Number IN111601 and CONACYT Project Number 41209-F.

References

Abramowitz, M., and I. A. Stegun (1972). *Handbook of Mathematical Functions with Formulas, Graphs and Mathematical Tables*, Dover Publications Inc., New York.

Anderson, J. G., S. K. Singh, J. M. Espíndola, and J. Yamamoto (1989). Seismic strain release in the Mexican Subduction thrust, *Phys. Earth Planet. Interiors* **58,** 307–322.

Astiz, L., and H. Kanamori (1984). An earthquake doublet in Ometepec, Guerrero, Mexico, *Phys. Earth Planet. Interiors* **34,** 24–45.

Benjamin, J. R., and C. A. Cornell (1970). *Probability, Statistics and Decision for Civil Engineers*, McGraw Hill, Mexico (in Spanish).

Courboulex, F., M. A. Santoyo, J. Pacheco, and S. K. Singh (1997). The 14 September 1995 (M = 7.3) Copala, México earthquake: a source study using teleseismic, regional, and local data, *Bull. Seism. Soc. Am.* **87,** 999–1101.

Deng, J., and L. R. Sykes (1997). Evolution of the stress field in southern California and triggering of moderate-size earthquakes: a 200-year perspective, *J. Geophys. Res.* **102,** 9859–9886.

Freed, A. M., and J. Lin (1998). Time dependent changes in failure stress following thrust earthquakes, *J. Geophys. Res.* **103,** 24,393–24,409.

Gomberg, J., N. M. Beeler, M. L. Blanpied, and P. Bodin (1998). Earthquake triggering by transient and static deformations, *J. Geophys. Res.* **103,** 24,411–24,416.

Hardebeck, J., J. Nazareth, and E. Hauksson (1998). The static stress change triggering model: constraints from two southern California aftershock sequences, *J. Geophys. Res.* **103,** 24,427–24,437.

Harris, R. (1998). Introduction to special section: stress triggers, stress shadows, and implications for seismic hazards, *J. Geophys. Res.* **103,** 24,347–24,358.

Havskov, J., S. K. Singh, E. Nava, T. Domínguez, and M. Rodríguez (1983). Playa Azul, Michoacan, Mexico earthquake of 25 October (Ms = 7.3) 1981, *Bull. Seism. Soc. Am.* **73,** 449–457.

Kagan, Y., and D. D. Jackson (1991). Long-term earthquake clustering, *Geophys. J. Int.* **104,** 117–133.

Kagan, Y., and L. Knopoff (1976). Statistical search for non-random features of the seismicity of strong earthquakes, *Phys. Earth Planet. Interiors* **12,** 291–318.

King, G. C. P., R. S. Stein, and J. Lin (1994). Static stress changes and the triggering of earthquakes, *Bull. Seism. Soc. Am.* **84,** 935–953.

Kostoglodov, V., and J. Pacheco (1999). Cien años de sismicidad en México, Instituto de Geofisica, UNAM (poster).

Mendoza, X., and X. Hartzell (1989). Slip distribution of the 19 September 1985 Michoacan, Mexico, earthquake: near-source and teleseismic constraints, *Bull. Seism. Soc. Am.* **79,** 655–669.

Mikumo, T., S. K. Singh, and M. A. Santoyo (1999). A possible stress interaction between large thrust and normal faulting earthquakes in the mexican subduction zone, *Bull. Seism. Soc. Am.* **89,** 1418–1427.

Mikumo, T., Y. Yagi, S. K. Singh, and M. A. Santoyo (2002). Coseismic and postseismic stress changes in a subducting plate: possible stress interactions between large interplate thrust and intraplate normal faulting earthquakes, *J. Geophys. Res.* **107,** no. B1, ESE5-1 to ESE5-12.

Nishenko, S. P., and S. K. Singh (1987a). Conditional probabilities for the recurrence of large and great interplate earthquakes along the Mexican subduction zone, *Bull. Seism. Soc. Am.* **77,** 2095–2114.

Nishenko, S. P., and S. K. Singh (1987b). The Acapulco-Ometepec, Mexico, earthquakes of 1907–1982: evidence for a variable recurrence history, *Bull. Seism. Soc. Am.* **77,** 1359–1367.

Ortiz, M., S. K. Singh, V. Kostoglodov, and J. Pacheco (2000). Source areas of the Acapulco-San Marcos, Mexico earthquakes of 1962 (M 7.1, 7.0) and 1957 (M 7.7), as constrained by Tsunami and uplift records, *Geofísica Internacional* **39,** no. 4, 337–348.

Okada, Y. (1985). Surface deformation due to shear and tensile faults in a half space, *Bull. Seism. Soc. Am.* **75,** 1135–1154.

Okada, Y. (1992). Internal deformation due to shear and tensile faults in a half space, *Bull. Seism. Soc. Am.* **82,** 1018–1040.

Pacheco, J., S. K. Singh, J. Dominguez, A. Hurtado, L. Quintanar, Z. Jimenez, J. Yamamoto, C. Gutierrez, M. A. Santoyo, W. Bandy, M. Guzman, and V. Kostoglodov (1997). The October 9, 1995 Colima-Jalisco, Mexico, earthquake (M_w 8): an aftershock study and a comparison of this earthquake with those of 1932, *Geophys. Res. Lett.* **24,** 2223–2226.

Purcaru, G., and H. Berckhemer (1978). Quantitative relations of seismic source parameters and a classification of earthquakes, *Tectonophysics* **84,** 57–128.

Reyes, A., J. N. Brune, and C. Lomnitz (1979). Source mechanism and aftershock study of the Colima, Mexico earthquake of January 10, 1973, *Bull. Seism. Soc. Am.* **69,** 1819–1840.

Santoyo, M. A. (1994). Estudio del proceso de ruptura del sismo del 25 de abril de 1989 usando registros de movimientos fuertes y telesísmicos, M.S. Thesis, UACPYP-CCH, Universidad Nacional Autónoma de México (UNAM) (in Spanish).

Singh, S. K., and F. Mortera (1991). Source-time functions of large Mexican subduction earthquakes, morphology of the Benioff zone, and the extent of the Guerrero gap, *J. Geophys. Res.* **96,** 21,487–21,502.

Singh, S. K., L. Astiz, and J. Havskov (1981). Seismic gaps and recurrence periods of large earthquake along the Mexican subduction zone: a reexamination, *Bull. Seism. Soc. Am.* **71,** 827–843.

Singh, S. K., J. Havskov, K. McNally, L. Ponce, T. Hearn, and M. Vassiliou (1980). The Oaxaca Mexico earthquake of 29 November 1978: a preliminary report on aftershocks, *Science* **207,** 1211–1213.

Singh, S. K., J. F. Pacheco, L. Alcantara, G. Reyes, M. Ordaz, A. Iglesias, S. M. Alcocer, C. Gutierrez, C. Valdés, V. Kostoglodov, C. Reyes, T. Mikumo, R. Quaas, and J. G. Anderson (2003). A preliminary report on the Tecomán, México, earthquake of 22 January 2003 (Mw 7.4) and its effects, *Seism. Res. Lett.* **74,** 279–289.

Singh, S. K., L. Ponce, and S. P. Nishenko (1985). The great Jalisco, Mexico, earthquakes of 1932: subduction of the rivera plate, *Bull. Seism. Soc. Am.* **75,** 1301–1313.

Singh, S. K., M. Rodríguez, and J. M. Espíndola (1984). A catalog of shallow earthquakes of Mexico from 1900 to 1981, *Bull. Seism. Soc. Am.* **74,** 267–279.

Stein, S. (1999). The role of stress transfer in earthquake occurrence, *Nature* **402,** 605–609.

Stein, R. S., G. C. P. King, and J. Lin (1994). Stress triggering of the 1994 M = 6.7 Northridge, California earthquake by its predecesors, *Science* **265,** 1432–1435.

Toda, S., R. S. Stein, P. A. Reasenberg, J. H. Dieterich, and A. Yoshida (1998). Stress transferred by the 1995 Mw = 6.9 Kobe, Japan, shock: effect on aftershocks and future earthquake probabilities, *J. Geophys. Res.* **103,** 24,543–24,565.

Universidad Nacional Autónoma de México (UNAM) Seismology Group (1986). The September 1985 Michoacan earthquakes: aftershock distribution and history of rupture, *Geophys. Res. Lett.* **13,** 573–576.

Utsu, T., and A. Seki (1954). A relation between the area of aftershock region and the energy of mainshock, *J. Seism. Soc. Jap.* **7,** 233–240.

Valdés, C., and D. Novelo (1998). The western Guerrero, Mexico, seismogenic zone from the microseismicity associated to the 1979, Petatlán and 1985, Zihuatanejo earthquakes, *Tectonophysics* **287,** 271–277.

Ward, S. N. (1992). An application of synthetic seismicity calculations in earthquake statistics: the middle America trench, *J. Geophys. Res.* **97,** 6675–6682.

Wells, D. L., and K. J. Coppersmith (1994). New empirical relationships among magnitude, rupture length, rupture width, rupture area, and surface displacement, *Bull. Seism. Soc. Am.* **84,** 974–1002.

Yagi, Y., T. Mikumo, J. Pacheco, and G. Reyes (2004). Source rupture process of the Tecomán, Colima, Mexico earthquake of 22 January 2003, determined by joint inversion of teleseismic body-wave and near-source data, *Bull. Seism. Soc. Am.* **94,** 1795–1807.

Zuñiga, F. R., and M. Wyss (2001). Most- and least-likely locations of large to great earthquakes along the pacific coast of Mexico estimated from local recurrence times based on *b*-values, *Bull. Seism. Soc. Am.* **91,** 1717–1728.

Zúñiga, F. R., C. Gutierrez, E. Nava, J. Lermo, M. Rodriguez, and R. Coyoli (1993). Aftershocks of the San Marcos, earthquake, of April 25, 1989 and its implications for the potential of the Acapulco-San Marcos region, *Pure Appl. Geophys.* **140,** 287–300.

Appendix

To ensure that our method would not identify an unclustered dataset as a clustered one, we performed the following test: we generated a large number of synthetic catalogs with the same magnitude exceedence rate characteristics (expected number of earthquakes per unit time) of the actual one, but with a known Poissonian behavior in time, and applied our method to them. We then, checked how many synthetic catalogs produced a possible non-Poissonian behavior, according to our algorithm. To do this we generated 10,000 catalogs, where for each catalog we assigned the following characteristics:

1. Following a Poissonian model, the interevent times (termed as interarrival times by Benjamin and Cornell, 1970), were assigned an exponential distribution, with the same value of $\lambda = 46/103 = 0.447$ (event/year) as the actual catalog. To simulate the interevent times we used

$$\tau_i = -\left(\frac{1}{\lambda}\right) \ln(u_i),$$

where τ_i = interevent time, u_i is a uniformly distributed random number between 0 and 1, and

$$T_i = \sum_{k=1}^{i} \tau_k$$

is the time of occurrence of each earthquake in the synthetic catalog.

2. The spatial location along the trench of each earthquake was set following a uniform distribution $x_i = 1350\ u_i$, where u_i is again a uniformly distributed random number between 0 and 1.

3. For the magnitude distribution of events in the catalog, we assigned a truncated Gaussian distribution with $E_m = 7.03$ and $\sigma = 0.84$, which are the mean and standard deviation values for this distribution, obtained from the actual catalog. Then, $M_i = E_m + \sigma y_i$, $6.8 \leq M_i \leq 8.2$, where M_i is the magnitude assigned to each event and y_i is a random number with standard normal distribution. Then, the DEI for each event was assigned according to the relation $\log(S) = M - 4.1$ and $L = 2W$. Finally, we applied the method to each synthetic catalog.

From this test, our method concluded that only 512 out of the 10,000 synthetic catalogs (5.12%) behaved as non-Poissonian, and 94.88% of the cases behaved as Poissonian, indicating that our method is working with a good confidence level and that it is very unlikely that an unclustered dataset could be identified as clustered by our algorithm.

Another test performed was to assure that a change of 15% in the length of the DEI length due to the different distribution of slips, would not significantly affect the results of the statistical analysis. Here we changed this length in three different ways: We (1) increased by 15% the values of DEI of all the earthquakes on the catalog and applied our method; (2) reduced by 15% the DEI values of all earthquakes on the catalog, and again applied the method, and (3) generated a random 15% increase or decrease of the DEI for each earthquake on the catalog and applied the method in 100 different runs. In all cases (100%), the tests yielded no evidence to favor the Poisson hypothesis of earthquake occurrence.

Instituto de Geofísica
Universidad Nacional Autónoma de México (UNAM)
Circuito Institutos s/n, Ciudad Universitaria
Coyoacán, 04510
México, D.F., México
(M.A.S., S.K.S, T.M.)

Instituto de Ingeniería
Universidad Nacional Autónoma de México (UNAM)
Circuito Institutos s/n, Ciudad Universitaria
Coyoacán, 04510
México, D.F., México
(M.O.)

Manuscript received 20 September 2004.